Applied Physics Letters

RESEARCH ARTICLE | JUNE 01 2023

Radiative volume plasmon and phonon-polariton resonances in TiN-based plasmonic/polar-dielectric hyperbolic optical metamaterials

Krishna Chand Maurya; Vincenzo Caligiuri; Ashalatha Indiradevi Kamalasanan Pillai; ... et. al

Check for updates

Appl. Phys. Lett. 122, 221704 (2023)
https://doi.org/10.1063/5.0150185

View Online
Export Citation
CrossMark

Articles You May Be Interested In

Schottky barrier height of epitaxial lattice-matched TiN/$Al_{0.72}Sc_{0.28}N$ metal/semiconductor superlattice interfaces for thermionic energy conversion

Appl. Phys. Lett. (December 2019)

Ferroelectric behavior of sputter deposited $Al_{0.72}Sc_{0.28}N$ approaching 5 nm thickness

Appl. Phys. Lett. (June 2023)

Electrical breakdown strength enhancement in aluminum scandium nitride through a compositionally modulated periodic multilayer structure

Journal of Applied Physics (October 2021)

QBLOX
Integrates all
Instrumentation + Software
for Control and Readout of
Superconducting Qubits
NV-Centers
Spin Qubits

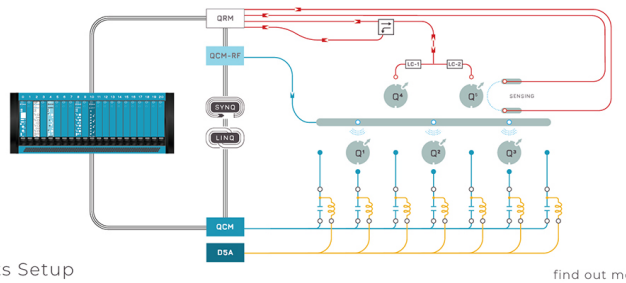

Spin Qubits Setup
find out more >

AIP Publishing

Downloaded from http://pubs.aip.org/aip/apl/article-pdf/doi/10.1063/5.0150185/17925374/221704_1_5.0150185.pdf

Applied Physics Letters ARTICLE pubs.aip.org/aip/apl

Radiative volume plasmon and phonon-polariton resonances in TiN-based plasmonic/polar-dielectric hyperbolic optical metamaterials

Cite as: Appl. Phys. Lett. **122**, 221704 (2023); doi: 10.1063/5.0150185
Submitted: 13 March 2023 · Accepted: 19 May 2023 ·
Published Online: 1 June 2023

View Online Export Citation CrossMark

Krishna Chand Maurya,[1,2] Vincenzo Caligiuri,[3] Ashalatha Indiradevi Kamalasanan Pillai,[4] Magnus Garbrecht,[4] Roman Krahne,[5] and Bivas Saha[1,2,6,a)]

AFFILIATIONS

[1]Chemistry and Physics of Materials Unit, Jawaharlal Nehru Centre for Advanced Scientific Research, Bangalore 560064, India
[2]International Centre for Materials Science, Jawaharlal Nehru Centre for Advanced Scientific Research, Bangalore 560064, India
[3]Dipartimento di Fisica, Università della Calabria, Rende 87036, Italy
[4]Sydney Microscopy & Microanalysis, The University of Sydney, Camperdown, NSW 2006, Australia
[5]Optoelectronics Research Line, Istituto Italiano di Tecnologia, Via Morego 30, Genova 16163, Italy
[6]School of Advanced Materials, Jawaharlal Nehru Centre for Advanced Scientific Research, Bangalore 560064, India

[a)]Author to whom correspondence should be addressed: bsaha@jncasr.ac.in and bivas.mat@gmail.com

ABSTRACT

Ferrell and Berreman modes are absorption resonances in thin metal films and polar-dielectric media that arise from radiative bulk plasmon-polariton and phonon-polariton excitations. Compared to surface polaritons, Ferrell and Berreman modes occur due to volume charge oscillations across the medium and provide a unique pathway for light–matter interactions. Though the resonances are studied individually, stringent polarization and material requirements have prevented their observation in one host medium. Here, we show simultaneous excitation of Ferrell and Berreman absorption resonances in refractory epitaxial TiN/$Al_{0.72}Sc_{0.28}N$ plasmonic metal/polar-dielectric hyperbolic metamaterials in the visible and far-infrared spectral ranges. The nanoscale periodicity of the superlattices enables the coupling of bulk plasmons (and longitudinal optical phonons) across different TiN (and $Al_{0.72}Sc_{0.28}N$) layers and allows polarization matching with free-space light that results in Ferrell (and Berreman) mode excitations. Ferrell and Berreman absorption resonances can be used for strong light confinement in radiative cooling, thermophotovoltaics, and other dual-band applications.

Published under an exclusive license by AIP Publishing. https://doi.org/10.1063/5.0150185

Plasmons are quantized quasiparticles that represent the collective (plasma) oscillation of the free electron gas density.[1] Plasma oscillation in metals is longitudinal, where electron motion and plasma movement follow the same direction. On the other hand, free-space propagating light is a transverse wave. Due to this polarization mismatch, electromagnetic waves do not couple with the plasma oscillations. However, at the surface of thin metallic foils, image forces constraint electrons to remain inside the metal, which leads to an uncertainty in the momentum perpendicular to the foil.[2] As a result, the plasma oscillation acquires a transverse character and couples with *p*-polarized light at oblique incidence, which produces resonances known as the Ferrell modes[2] [see Fig. 1(a)]. Unlike surface plasmon polaritons that are dark and correspond to the charge oscillations on metal surfaces, Ferrell modes result from the volume charge oscillation across the metal foil and are radiative.[3] Due to the sharp and intense resonance, Ferrell absorption can be used for applications such as polarization control,[4] sensing,[5] imaging,[6] and solar energy harvesting.[7]

Similar to the Ferrell modes, ultrathin polar-dielectric materials also exhibit a sharp and strong IR absorption band close to their longitudinal optical (LO) phonon frequencies, referred to as the Berreman mode[8] [see Fig. 1(b)]. These leaky TM (transverse magnetic)-polarized polaritonic resonances[9] originate spectrally close to the LO phonon in ultrathin polar-dielectric media and acquire transverse character due to the coupling between top and bottom interfaces. Berreman resonances provide an effective way to achieve strong light–matter interactions in the (far)-IR spectral regime and could be useful in thermal

Downloaded from http://pubs.aip.org/aip/apl/article-pdf/doi/10.1063/5.0150185/17925374/221704_1_5.0150185.pdf

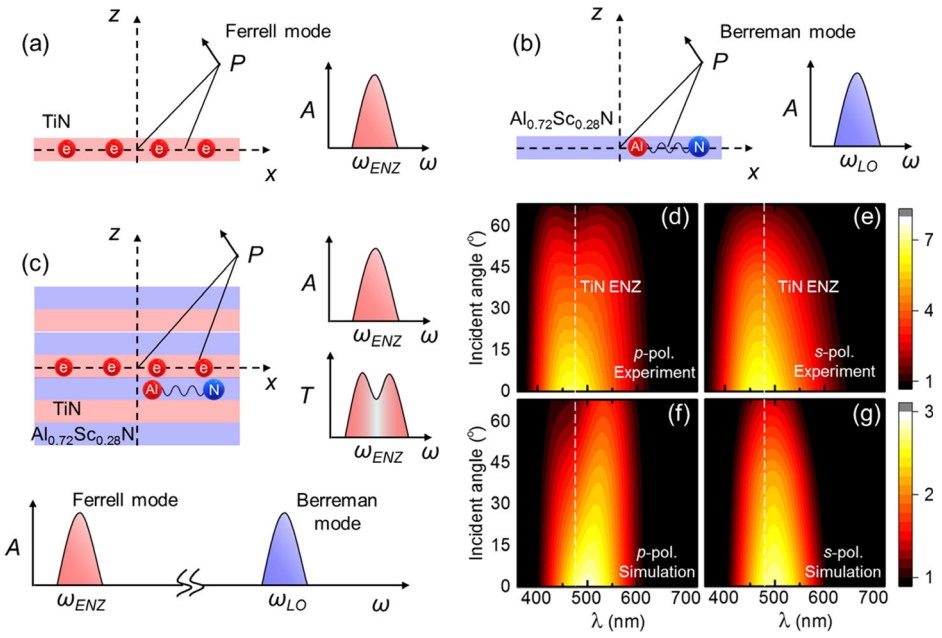

FIG. 1. Excitation of Ferrell and Berreman modes in TiN/$Al_{0.72}Sc_{0.28}N$ metal/polar-dielectric superlattices. (a) Schematic of Ferrell absorption on a thin metallic film close to its epsilon-near-zero frequency (ω_{ENZ}). (b) Schematic of Berreman absorption on a thin polar dielectric close to its LO phonon frequency. (c) Schematic of Ferrell and Berreman absorption in a metal/polar-dielectric superlattice. Ferrell modes in superlattice appear due to absorptions from radiative bulk plasmon-polariton mode, while Berreman mode appears due to the coupling of light with LO phonon-polariton in $Al_{0.72}Sc_{0.28}N$. Experimentally measured transmission spectra of (d) *p*-polarized and (e) *s*-polarized light through a 20 nm/20 nm TiN/$Al_{0.72}Sc_{0.28}N$ metal/dielectric superlattice. The dip in absorption at ∼470 nm in *p*-polarized transmission corresponds to the Ferrell absorption. No such transmission dip is observed in *s*-polarized light. Simulated (f) *p*-polarized and (g) *s*-polarized transmission spectra calculated with the transfer matrix approach (the finite element method, see supplementary material Fig. S5) showing the Ferrell absorption.

emitters,[10] passive radiative cooling,[11] diagnosis tools for cancer detection,[12] biomolecular fingerprinting,[13] etc.

Ferrell and Berreman absorption have usually been studied separately in thin metals and polar-dielectric films. For example, electron beam irradiation[3,14] has been used to study the Ferrell modes in elemental metals such as Ag, Au, Cu, Al, and Ti.[15,16] In contrast, alkali halides such as LiF[8] and well-established polar dielectrics such as AlN,[17] GaN,[18,19] and SiC[20] are used to excite the Berreman modes.[9] The narrow-band Berreman resonance in AlN has also been proposed as a selective thermal emitter.[10] Furthermore, active tuning of the Berreman modes with LO phonon-plasmon coupling and embedded eigenstates based on Berreman modes have been demonstrated.[21] However, the development of dual-band absorbers hosting both Ferrell and Berreman modes is yet to be demonstrated due to the conflicting material and optical property requirements. Several emerging technologies often demand for large absorbance in both the UV-VIS and the near IR spectral range.[22–25] To accomplish such a task, the so-called "metamaterials" offer unparalleled design opportunity.[26–29]

The necessity of having plasmonic and polar-dielectric materials in one meta-structure can be obtained in epitaxial plasmonic metal/polar-dielectric superlattices [see Fig. 1(c)]. However, most demonstrations of metal/dielectric multilayers involve Au or Ag as plasmonic components and amorphous dielectric such as SiO_2 and TiO_2 that exhibit covalent character.[7,30] Moreover, due to the significant surface energy mismatches, the multilayers mentioned earlier generally do not possess atomically sharp and abrupt interfaces, leading to additional complexity in analyzing their properties. Nevertheless, Ferrell modes have been recently demonstrated in Ag/SiO_2 metal/dielectric multilayers.[31] However, due to the covalent nature of SiO_2, achieving polar phonon modes and Berreman excitation in such multilayers is challenging.

The dual-band Ferrell and Berreman absorption can be achieved in TiN/$Al_{0.72}Sc_{0.28}N$ metal/polar-dielectric superlattices. TiN is a refractory transition-metal nitride, exhibits an epsilon-near-zero (ENZ) resonance at ∼470 nm, and is regarded as an alternative plasmonic material to gold. TiN exhibits a high melting temperature of 2600 °C, is corrosion resistant, shows a high mechanical hardness of 24 GPa, and can be deposited in thin film and ultrathin film form.[32,33] Similarly, rock salt-$Al_{0.72}Sc_{0.28}N$ is a polar dielectric developed with the solid-state alloying of AlN and ScN to lattice-match with TiN.[34] AlN17 and ScN[35,36] are polar semiconductors, and rock salt-$Al_{0.72}Sc_{0.28}N$ exhibits a LO phonon frequency at 848 cm^{-1} close to the LO phonon frequency of AlN. Epitaxial TiN/$Al_{0.72}Sc_{0.28}N$ superlattices show hyperbolic photonic dispersion with both type-I and type-II characteristics[34] and significantly high densities of photonic states. Plasmonic properties of TiN/$Al_{0.72}Sc_{0.28}N$ multilayers with varying dielectric thicknesses have been observed and discussed recently.[37] As TiN's plasmonic properties vary with the mechanical strain present in the film,[38] achieving lattice-matched interfaces of TiN with $Al_{0.72}Sc_{0.28}N$ is crucial for achieving the high-quality Ferrell modes. In this work, we demonstrate the coexistence of both Ferrell and Berreman absorption resonances in refractory CMOS-compatible and

Downloaded from http://pubs.aip.org/aip/apl/article-pdf/doi/10.1063/5.0150185/17925374/221704_1_5.0150185.pdf

Published under an exclusive license by AIP Publishing

epitaxial TiN/$Al_{0.72}Sc_{0.28}N$ metal/polar-dielectric superlattices with nanoscale layer thicknesses that translate to nanoscale periodicity.

TiN/$Al_{0.72}Sc_{0.28}N$ superlattices with periodicity of 40 nm (20 nm/20 nm, eight periods), 20 nm (10 nm/10 nm, eight periods), and 10 nm (5 nm/5 nm, 16 periods) are deposited on double-side polished (001) MgO substrates with ultrahigh-vacuum DC-magnetron sputtering at a base pressure of 1×10^{-9} Torr. Additionally, 80 nm TiN and 100 nm $Al_{0.72}Sc_{0.28}N$ films are deposited on (001) MgO and on 100 nm TiN coated (001) MgO substrates, respectively. TiN coating on MgO substrates serves as metallic back plates. Details about the growth and material characterization are presented in supplementary material sections 1–3.

Angle- and polarization-dependent transmission measurements of 40 nm period superlattices show a dip in the transmission at ~470 nm for the *p*-polarized light at oblique angles of incidence [see Fig. 1(d)]. At less than 30° angles of incidence, the transmission dip is less pronounced. This *p*-polarization transmission dip corresponds to the Ferrell mode close to TiN's epsilon-near zero (ENZ) frequency. Due to their radiative nature, Ferrell modes allow for light absorption at the ENZ frequency of the metal, which results in a dip in the *p*-polarized transmission spectrum. No such dip is observed for the *s*-polarization [see Fig. 1(e)] at any angle of incidence.

To investigate the origin of the transmission dip further, the dielectric permittivity of the superlattices is measured with spectroscopic ellipsometry. Results show that TiN layers exhibit a zero crossing of the real component of the dielectric permittivity (ε_1) at ~470 nm that corresponds to its ENZ wavelength [see Fig. 2(a)]. This transition is consistent with the dielectric-to-metallic crossover of a thick TiN film (80 nm thickness) that occurs at 2.637 eV (~470 nm see Fig. S4 in the supplementary material). On the other hand, $Al_{0.72}Sc_{0.28}N$ exhibits a dielectric optical response with real dielectric permittivity (ε_1) close to 5.5 throughout the visible-to-near IR spectral ranges [see Fig. 2(b)], which agrees well with the direct bandgap of $Al_{0.72}Sc_{0.28}N$ of ~3.4 eV.[39]

While the individual layers act as metallic and dielectric, the considered superlattice behaves as an effective anisotropic hyperbolic optical medium with different in-plane ($\varepsilon^{\parallel}$) and out-of-plane ($\varepsilon^{\perp}$) dielectric permittivity in the principal component of the dielectric tensor ($\overline{\overline{\varepsilon_{eff.}}}$) [see Eqs. (1) and (2)]. The anisotropic dielectric permittivity determined with the first-order Maxwell Garnett effective medium theory [see Eqs. (3) and (4)][29] shows that, consistent with previous reports,[34] TiN/$Al_{0.72}Sc_{0.28}N$ superlattices exhibit a hyperbolic photonic dispersion with different signs of the $\varepsilon_1^{\parallel}$ and $\varepsilon_1^{\perp}$ [see Fig. 2(c)]. From 490 to 605 nm, $\varepsilon_1^{\parallel}$ is positive, while $\varepsilon_1^{\perp}$ is negative, leading to a so-called type-I hyperbolic dispersion. However, beyond 605 nm, the permittivities reverse their sign, leading to a type-II hyperbolic dispersion. Consistent with its hyperbolic photonic nature, the imaginary part of the dielectric permittivity along the out-of-plane direction ($\varepsilon_2^{\perp}$) exhibits [see Fig. 2(d)] a peak at the epsilon-near-pole resonance (ENP), as a signature of the type-I-to-type-II iso-frequency or Lifshitz transition,[40]

$$\varepsilon = \varepsilon_1 + i\varepsilon_2, \tag{1}$$

$$\overline{\overline{\varepsilon_{eff.}}} = \mathrm{diag}\,[\varepsilon^{\parallel}, \varepsilon^{\parallel}, \varepsilon^{\perp}], \tag{2}$$

$$\varepsilon^{\parallel} = \rho\varepsilon_m + (1-\rho)\varepsilon_d, \tag{3}$$

$$\varepsilon^{\perp} = \left(\rho/\varepsilon_m + (1-\rho)/\varepsilon_d\right)^{-1}. \tag{4}$$

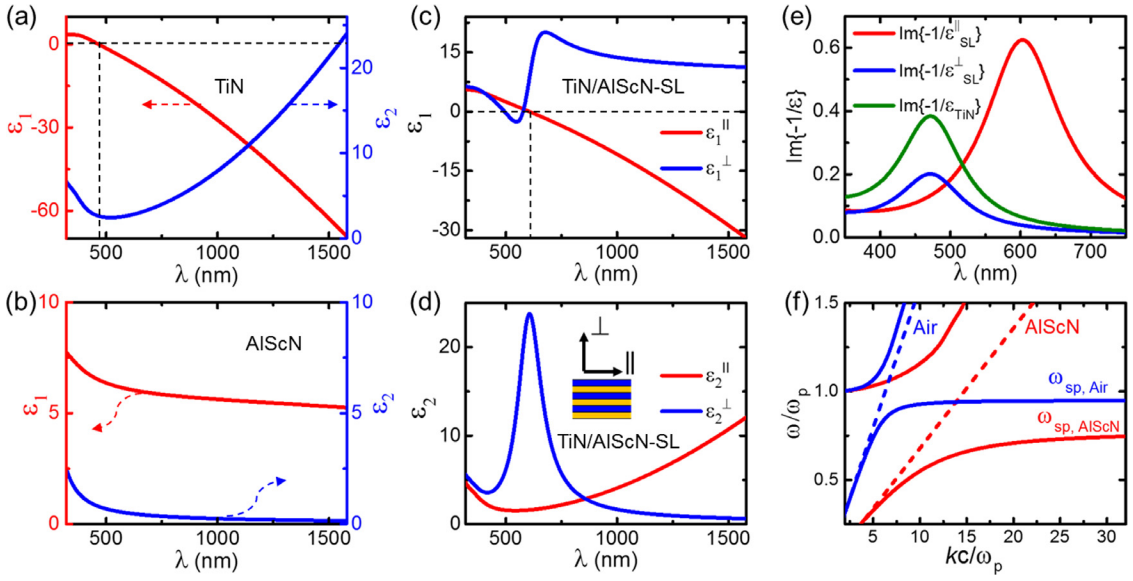

FIG. 2. Dielectric permittivity of TiN, $Al_{0.72}Sc_{0.28}N$, and TiN/$Al_{0.72}Sc_{0.28}N$ metal/dielectric superlattice hyperbolic metamaterials. (a) Real and imaginary components of the dielectric permittivity of TiN inside the superlattice (extracted from spectroscopic ellipsometry measurements) are presented. TiN exhibits an epsilon-near-zero (ENZ) wavelength at ~470 nm. (b) The dielectric constant of r-$Al_{0.72}Sc_{0.28}N$ inside the superlattice is extracted similarly. (c) Anisotropic dielectric constant of TiN/$Al_{0.72}Sc_{0.28}N$ metal/semiconductor superlattices calculated with the effective medium approximation. $\varepsilon_1^{\parallel}$ and $\varepsilon_1^{\perp}$ represent the real component of the permittivity along the in-plane and out-of-plane directions, respectively. Both type-I and type-II hyperbolic photonic dispersions are achieved from 490 to 605 nm and from 605 to 1500 nm, respectively. (d) Imaginary component of the dielectric permittivity of the superlattices shows a high optical loss in $\varepsilon_2^{\perp}$ at 605 nm. (e) The energy-loss function $Im\{-1/\varepsilon\}$ for TiN film (green curve), for superlattice in-plane (red curve), and out-of-plane (blue curve). (f) Dispersion relation of SPPs at the interface between TiN with air (blue curves) and $Al_{0.72}Sc_{0.28}N$ (red curves) along with the light lines (dotted lines).

Downloaded from http://pubs.aip.org/aip/apl/article-pdf/doi/10.1063/5.0150185/17925374/221704_1_5.0150185.pdf

Published under an exclusive license by AIP Publishing

Here, $\overline{\overline{\varepsilon_{eff.}}}$ is the dielectric permittivity tensor of the superlattice that constitutes a hyperbolic optical medium. ε_m and ε_d are the complex dielectric permittivities of the metal (TiN) and dielectric ($Al_{0.72}Sc_{0.28}N$) layers, respectively, and $\rho = \frac{d_m}{d_m+d_d}$ corresponds to the metal volume fill fraction, where d_m and d_d are the thicknesses of the metal and dielectric layers, respectively.

From the knowledge of the dielectric permittivity of the individual layers and the superlattices, it is clear that the dip in the *p*-polarization transmission occurs at the ENZ wavelength of TiN and cannot be traced back to any ENZ, ENP, or interband transition of the superlattices. For interband transitions, the absorption should have been observable for both the polarization states. The *p*-polarization transmittance dip can be directly connected to the sharp maxima of the energy-loss function $Im\{-1/\varepsilon^{\perp}(\omega)\}$ of TiN, as shown in Fig. 2(e). The absence of such a dip in the transmission spectra of an 80 nm thick TiN film in either *p*- or *s*-polarization [see Fig. 3(a)] confirms the radiative volume plasmon-polariton nature of this resonance that appears as a Ferrell mode in the superlattices due to the presence of thin TiN. Indeed, since volume charge oscillations in bulk TiN (thick films) are purely longitudinal, they cannot be excited with the free-space light. Similarly, surface plasmon-polariton excitation modes at the TiN/$Al_{0.72}Sc_{0.28}N$ interfaces fall below to the right of the light cone and, therefore, cannot be excited [see Fig. 2(f)].

Transmission measurements carried out on the other TiN/$Al_{0.72}Sc_{0.28}N$ superlattices (with 40, 20, and 10 nm periodicity) also show the *p*-polarization transmission dip at 470 nm at high angles of incidence, and no transmission dip for the *s*-polarized light [see Figs. 3(b) and 3(d)]. The dispersion-less nature of the dip, whose spectral position remains unvaried while increasing the incidence angle, is a further proof that it is a Ferrell mode rather than a Fabry–Pérot one.[41]

The mechanism of the Ferrell mode excitation in superlattices has a slightly different physical origin than that of an isolated ultrathin metal foil. Since the thicknesses of individual TiN layers inside the superlattice are smaller than the optical skin depth (~40–50 nm),[42] volume charge oscillations across different interfaces couple with each other and lead to a collective charge oscillation across the superlattice. Therefore, the collective volume charge oscillation acquires a transverse character that enables its interaction with free-space light. According to the calculation of McAlister and Stern,[43] the decay rate (inverse of radiative mean lifetime) of the Ferrell mode is strongly dependent on the angle of incidence, through the relation

$$\tau_r^{-1} \approx \frac{2}{\varepsilon'}\frac{\pi d}{\lambda}\sin\theta\tan\theta \approx \omega_p \frac{\pi d}{\lambda}\sin\theta\tan\theta, \quad (5)$$

where τ_r is the radiative mean lifetime, θ is the angle of incidence measured from the film normal, λ is the wavelength, d is the thickness of the film, and $\varepsilon' = \left(\frac{d\varepsilon_m}{d\omega}\right)_{\omega=\omega_p}$ measured at the plasma frequency. Equation (5) suggests an extremely fast decay rate for the radiation that is caused by the high degree of correlation for the long wavelength plasmons. For an incident angle of 60° and 20 nm TiN thickness, the $\tau_r^{-1} \approx 0.198\omega_p$. Therefore, while the interband and other types of electronic transition usually exhibit a transition rate of $10^8\,s^{-1}$, the Ferrell mode exhibits a decay rate of a fraction of the plasma frequency of $\sim 10^{15}\,s^{-1}$.[2]

Equation (5) also shows that the width of the transmission dip (inverse of the lifetime) and its magnitude (strength of the absorption) are determined not only by the slope of the real part of the dielectric permittivity of the metal and the optical loss at the ENZ frequency, but also by the angle of incidence and thickness of the metal. The depth of the transmission dip and its width are calculated as a function of the angle of incidence in Fig. 4. The plot shows that the transmission dip (namely, the Ferrell absorption) is strongest when θ is ~50°–65°. The width of the transmission dip is also maximized at large angles of incidence at 60°–72° that supports the underlying physical mechanism. Furthermore, among the three superlattices studied here, the strength of the Ferrell absorption shows maximum intensity for the 20 nm periodicity (see Sec. 6 in the supplementary material).

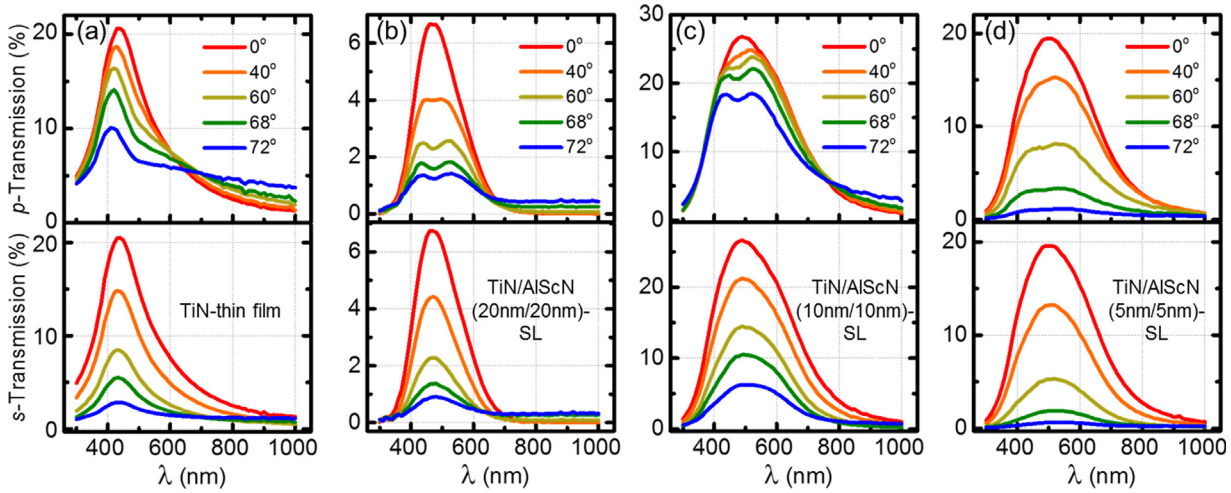

FIG. 3. Ferrell mode in TiN/$Al_{0.72}Sc_{0.28}N$ metal/dielectric superlattices as a function of superlattice periodicity. Polarized transmission measurements of (a) 80 nm thick TiN, (b) 20/20 nm, (c) 10/10 nm, and (d) 5/5 nm superlattices are presented. Superlattices show a dip in transmission for the *p*-polarized light at higher angle-of-incidence representative of the excitation of the Ferrell mode excitation. No such transmission dips are observed in the *s*-polarized light. 80 nm thick TiN does not exhibit any transmission dip, which is consistent with the fact that Ferrell modes cannot be excited in thicker films.

Downloaded from http://pubs.aip.org/aip/apl/article-pdf/doi/10.1063/5.0150185/17925374/221704_1_5.0150185.pdf

Published under an exclusive license by AIP Publishing

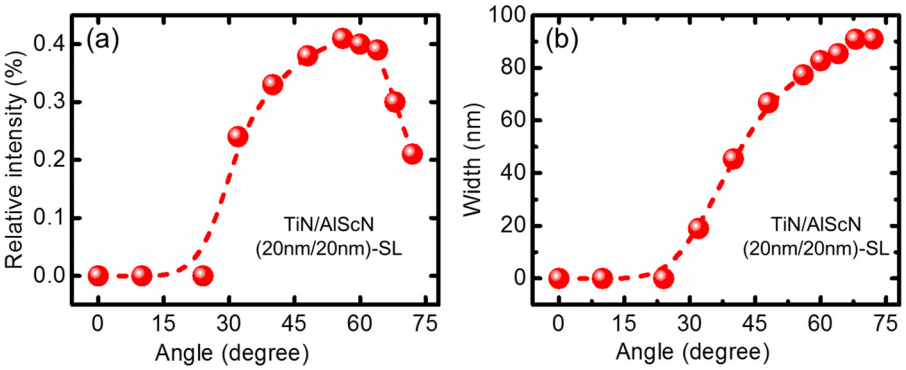

FIG. 4. Angle-dependence of Ferrell mode in TiN/$Al_{0.72}Sc_{0.28}N$ metal/dielectric superlattices. (a) Relative intensity (the amount of decrease in the transmission peak with respect to an undipped peak at the ENZ point) and (b) width [full-width-at-half-maxima (FWHM)] in 20/20 nm TiN/$Al_{0.72}Sc_{0.28}N$ metal/dielectric eight period superlattice as a function of angle of incidence. The intensity is higher for $\theta \sim 50°$–$65°$, while the width gradually increases with the angle.

The experimental transmission spectra are further modeled with transfer matrix approach (and the finite element method, see supplementary material Fig. S5) utilizing the dielectric permittivity values of the individual layers. As shown in Figs. 1(f) and 1(g), the calculated *p*-polarized and *s*-polarized transmissions look similar to the experimentally measured spectra with well-established dip in the transmission for *p*-polarized light. Though the amount of dip in the transmission spectrum and, consequently, the strength of Ferrell mode excitations are relatively low, further research on the reduction of metal thickness and variations of the number of superlattice periods and period thickness would lead to stronger Ferrell absorptions. Similarly, compared to the metasurfaces and metamaterials that often produce sharper resonances with larger Q-factor[44–47] but require costly nanofabrication and lithography processes, the present approach is easily scalable from the nano- to the wafer-scale since it is based on an intrinsic property of a material. Furthermore, the Ferrell mode spectral positions occur at the ENZ position of the plasmonic metal under investigation and do not depend on the size and shape of the nanostructures that would be useful for absorption at targeted spectral range applications.

Similar to the Ferrell mode excitation, reflectivity measurements of the 20/20 nm TiN/$Al_{0.72}Sc_{0.28}N$ superlattices [see Fig. 5(a)] show a sharp dip close to the LO phonon frequency of $Al_{0.72}Sc_{0.28}N$ layers at 848 cm^{-1} that represent the Berreman excitation.[48] The full-width-at-the-half-maxima (FWHM) of the Berreman absorption is 75 cm^{-1}, which results in a resonance *Q*-factor ($\omega/\Delta\omega$) of 11.3. As discussed before, Berreman excitation follows nearly the same physical origin as the Ferrell resonance, except that the Berreman modes represent polar optical phonon vibrations. The experimentally measured reflectivity spectrum in Fig. 5(a) is modeled with Fresnel's equation (see the supplementary material for details) accompanied by a Berreman term[8] [Eqs. (6) and (7)],

$$R_{Berreman} = \left[1 - 4\delta\left(\frac{Im\,(\varepsilon_{PD})}{Re\,(\varepsilon_{PD})^2 + Im\,(\varepsilon_{PD})^2}\right)\right], \quad (6)$$

where ε_{PD} represents the permittivity of $Al_{0.72}Sc_{0.28}N$ layers, given by

$$\varepsilon_{PD} = \varepsilon_\infty\left(1 + \frac{\omega_{LO}{}^2 - \omega_{TO}{}^2}{\omega_{TO}{}^2 - \omega^2 - i\omega\Gamma}\right). \quad (7)$$

Here, ω_{LO} (ω_{TO}) is the LO (TO) phonon frequency of *r*-$Al_{0.72}Sc_{0.28}N$, Γ is the damping of the phonons, and $\delta/2\pi$ is the thickness of the dielectric film, measured in vacuum wavelengths of the incident radiation. The modeled reflectivity spectrum matches with the experiment.

The dielectric permittivity, extracted from the fitting of the reflectivity spectrum [see Fig. 5(b)], shows that the Berreman frequency appears close to the LO phonon frequency of $Al_{0.72}Sc_{0.28}N$ layers. At the LO phonon frequency, the dielectric permittivity of *r*-$Al_{0.72}Sc_{0.28}N$ exhibits an ENZ crossover, and the energy-loss function exhibits a sharp maximum [see Fig. 5(c)], both of which are necessary conditions for achieving the Berreman absorption. Similar to the superlattice with a 40 nm period thickness, the other two superlattices also show the similar Berreman excitations at the same spectral position as expected (see Sec. 7 in the supplementary material).

In conclusion, we demonstrate dual-band Ferrell and Berreman optical absorption in epitaxial plasmonic TiN/polar-semiconducting $Al_{0.72}Sc_{0.28}N$ hyperbolic metamaterials in the visible and far-infrared spectral ranges, respectively. The Ferrell and Berreman modes occur near the ENZ frequency of TiN and the longitudinal optical (LO) phonon frequency of $Al_{0.72}Sc_{0.28}N$, respectively. Their excitation with free-space light is enabled by the nanoscale thickness of the individual layers constituting the superlattice that allows for the collective

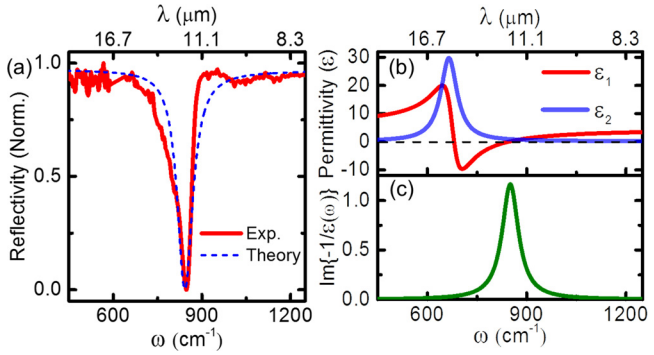

FIG. 5. Berreman modes in TiN/$Al_{0.72}Sc_{0.28}N$ metal/dielectric superlattices near the LO phonon frequency of r-$Al_{0.72}Sc_{0.28}N$. (a) A sharp decrease in reflectivity corresponding to the Berreman mode excitation (absorption) is shown on a 20 nm/20 nm TiN/$Al_{0.72}Sc_{0.28}N$ metal/dielectric superlattice. (b) Real and imaginary components of the dielectric permittivity of r-$Al_{0.72}Sc_{0.28}N$ in the far-infrared spectral range. Due to its polar-semiconducting nature, ε_1 of r-$Al_{0.72}Sc_{0.28}N$ exhibits a negative value within a band encompassed by the LO and TO phonon mode frequencies, known as the Reststrahlen band. (c) The energy-loss function $Im\{-1/\varepsilon\}$ for the r-$Al_{0.72}Sc_{0.28}N$ film.

Downloaded from http://pubs.aip.org/aip/apl/article-pdf/doi/10.1063/5.0150185/17925374/221704_1_5.0150185.pdf

Published under an exclusive license by AIP Publishing

excitation of volume plasmons across different interfaces. Such a mechanism endows these otherwise purely longitudinal waves with an additional degree of transverse behavior. Unlike the surface plasmon or phonon-polariton resonances, the Ferrell and Berreman excitations are radiative and are characterized by fast decay rates. Demonstration of the Ferrell and Berreman optical resonances in a single metamaterial marks a significant progress not only for the fundamental analysis of their physical properties, but also for the development of dual-band optical absorbers for solar-thermophotovoltaics, radiative cooling, and other nano-photonic applications.

See the supplementary material for the details on structural characterization of the superlattice, optical properties of TiN, details on the electromagnetic simulation method, angle-dependent reflection spectra, angle-dependence of Ferrell modes, and thickness dependence of Berreman modes in TiN/$Al_{0.72}Sc_{0.28}N$ superlattices.

K.C.M. and B.S. acknowledge International Centre for Materials Science (ICMS) and Sheikh Saqr Laboratory (SSL) in JNCASR for support. B.S. acknowledges the Young Scientist Research Award (YSRA) from the Board of Research in Nuclear Sciences (BRNS), Department of Atomic Energy (DAE), India with Grant No. 59/20/10/2020-BRNS/59020 for financial support. K.C.M. acknowledges Council of Scientific & Industrial Research (CSIR) for fellowship. M.G., A.I.K.P., and B.S. acknowledge the facilities of Sydney Microscopy & Microanalysis at The University of Sydney. V.C. acknowledges the research project "Componenti Optoelettronici Biodegradabili ed Eco-Sostenibili verso la nanofotonica green" (D.M. No. 1062, 10.08.2021, PON "Ricerca e Innovazione" 2014–2020) under contract identification code 1062_R17_GREEN.

AUTHOR DECLARATIONS

Conflict of Interest

The authors have no conflicts to disclose.

Author Contributions

Krishna Chand Maurya: Data curation (lead); Formal analysis (lead); Writing – original draft (lead). **Vincenzo Caligiuri:** Data curation (supporting); Validation (supporting); Writing – review & editing (supporting). **Ashalatha Indiradevi Kamalasanan Pillai:** Data curation (supporting); Validation (supporting); Writing – review & editing (supporting). **Magnus Garbrecht:** Data curation (supporting); Software (supporting); Writing – review & editing (supporting). **Roman Krahne:** Supervision (supporting); Validation (supporting); Writing – review & editing (supporting). **Bivas Saha:** Conceptualization (lead); Supervision (lead); Writing – review & editing (lead).

DATA AVAILABILITY

The data that support the findings of this study are available from the corresponding author upon reasonable request.

REFERENCES

[1]S. A. Maier, in *Plasmonics: Fundamentals and Applications* (Springer US, New York, 2007), pp. 39–52.
[2]R. A. Ferrell, Phys. Rev. **111**, 1214 (1958).
[3]W. Steinmann, Phys. Rev. Lett. **5**, 470 (1960).
[4]K. Y. Bliokh, F. J. Rodríguez-Fortuño, F. Nori, and A. V. Zayats, Nat. Photonics **9**, 796 (2015).
[5]R. A. Lewis, J. Phys. D: Appl. Phys. **52**, 433001 (2019).
[6]Z. Liu, H. Lee, Y. Xiong, C. Sun, and X. Zhang, Science **315**, 1686 (2007).
[7]C. F. Guo, T. Sun, F. Cao, Q. Liu, and Z. Ren, Light: Sci. Appl. **3**, e161 (2014).
[8]D. W. Berreman, Phys. Rev. **130**, 2193 (1963).
[9]I. Khan, Z. Fang, M. Palei, J. Lu, L. Nordin, E. L. Simmons, O. Dominguez, S. M. Islam, H. G. Xing, D. Jena, V. A. Podolskiy, D. Wasserman, and A. J. Hoffman, Opt. Express **28**, 28590 (2020).
[10]L. Nordin, O. Dominguez, C. M. Roberts, W. Streyer, K. Feng, Z. Fang, V. A. Podolskiy, A. J. Hoffman, and D. Wasserman, Appl. Phys. Lett. **111**, 091105 (2017).
[11]A. P. Raman, M. A. Anoma, L. Zhu, E. Rephaeli, and S. Fan, Nature **515**, 540 (2014).
[12]J. Verstockt, S. Verspeek, F. Thiessen, W. A. Tjalma, L. Brochez, and G. Steenackers, Sensors **22**, 3327 (2022).
[13]M. Huber, K. V. Kepesidis, L. Voronina, M. Božić, M. Trubetskov, N. Harbeck, F. Krausz, and M. Žigman, Nat. Commun. **12**(1), 1511 (2021).
[14]R. W. Brown, P. Wessel, and E. P. Trounson, Phys. Rev. Lett. **5**, 472 (1960).
[15]P. B. Johnson and R. W. Christy, Phys. Rev. B **6**, 4370 (1972).
[16]M. A. Ordal, L. L. Long, R. J. Bell, S. E. Bell, R. R. Bell, R. W. Alexander, and C. A. Ward, Appl. Opt. **22**, 1099 (1983).
[17]S. S. Ng, Z. Hassan, and H. Abu Hassan, Appl. Phys. Lett. **90**, 081902 (2007).
[18]K. C. Maurya, A. Chatterjee, S. M. Shivaprasad, and B. Saha, Nano Lett. **22**, 9606 (2022).
[19]V. Y. Davydov, Y. E. Kitaev, I. Goncharuk, A. Smirnov, J. Graul, O. Semchinova, and D. Uffmann, Phys. Rev. B **58**, 12899 (1998).
[20]R. Hillenbrand, T. Taubner, and F. Keilmann, Nature **418**, 159 (2002).
[21]A. D. Dunkelberger, D. C. Ratchford, A. B. Grafton, V. M. Breslin, E. S. Ryland, D. S. Katzer, K. P. Fears, R. J. Weiblen, I. Vurgaftman, A. J. Giles, C. T. Ellis, J. G. Tischler, J. D. Caldwell, and J. C. Owrutsky, ACS Photonics **7**, 279 (2020).
[22]C. C. Chang, W. J. M. Kort-Kamp, J. Nogan, T. S. Luk, A. K. Azad, A. J. Taylor, D. A. R. Dalvit, M. Sykora, and H. T. Chen, Nano Lett. **18**, 7665 (2018).
[23]M. Chirumamilla, A. Chirumamilla, Y. Yang, A. S. Roberts, P. K. Kristensen, K. Chaudhuri, A. Boltasseva, D. S. Sutherland, S. I. Bozhevolnyi, and K. Pedersen, Adv. Opt. Mater. **5**, 1700552 (2017).
[24]M. M. Hossain, B. Jia, and M. Gu, Adv. Opt. Mater. **3**, 1047 (2015).
[25]M. M. Hossain and M. Gu, Adv. Sci. **3**, 1500360 (2016).
[26]S. Jahani and Z. Jacob, Nat. Nanotechnol. **11**, 23 (2016).
[27]N. Kinsey, C. DeVault, A. Boltasseva, and V. M. Shalaev, Nat. Rev. Mater. **4**, 742 (2019).
[28]Z. Guo, H. Jiang, and H. Chen, J. Appl. Phys. **127**, 071101 (2020).
[29]D. Lee, S. So, G. Hu, M. Kim, T. Badloe, H. Cho, J. Kim, H. Kim, C.-W. Qiu, and J. Rho, ELight **2**(1), 1 (2022).
[30]K.-T. Lin, H. Lin, and B. Jia, Nanophotonics **9**, 3135 (2020).
[31]W. D. Newman, C. L. Cortes, J. Atkinson, S. Pramanik, R. G. Decorby, and Z. Jacob, ACS Photonics **2**, 2 (2015).
[32]R. V. Babinova, V. V. Smirnov, A. S. Useenov, K. S. Kravchuk, E. V. Gladkikh, V. I. Shapovalov, and I. L. Mylnikov, J. Phys.: Conf. Ser. **872**, 012035 (2017).
[33]X. Pang, L. Zhang, H. Yang, K. Gao, and A. A. Volinsky, J. Mater. Eng. Perform. **24**, 1185 (2015).
[34]B. Saha, G. V. Naik, S. Saber, C. Akatay, E. A. Stach, V. M. Shalaev, A. Boltasseva, and T. D. Sands, Phys. Rev. B **90**, 125420 (2014).
[35]K. C. Maurya, D. Rao, S. Acharya, P. Rao, A. I. K. Pillai, S. K. Selvaraja, M. Garbrecht, and B. Saha, Nano Lett. **22**, 5182 (2022).
[36]K. C. Maurya, B. Biswas, M. Garbrecht, and B. Saha, Phys. Status Solidi RRL **13**, 1900196 (2019).
[37]M. Garbrecht, L. Hultman, M. H. Fawey, T. D. Sands, and B. Saha, J. Mater. Sci. **53**, 4001 (2018).
[38]D. Shah, A. Catellani, H. Reddy, N. Kinsey, V. Shalaev, A. Boltasseva, and A. Calzolari, ACS Photonics **5**, 2816 (2018).
[39]B. Saha, S. Saber, G. V. Naik, A. Boltasseva, E. A. Stach, E. P. Kvam, and T. D. Sands, Phys. Status Solidi B **252**, 251 (2015).
[40]V. Caligiuri, R. Dhama, K. V. Sreekanth, G. Strangi, and A. De Luca, Sci. Rep. **6**, 20002 (2016).

Downloaded from http://pubs.aip.org/aip/apl/article-pdf/doi/10.1063/5.0150185/17925374/221704_1_5.0150185.pdf

Published under an exclusive license by AIP Publishing

[41]K. C. Maurya, A. I. K. Pillai, M. Garbrecht, and B. Saha, Mater. Today Phys. **27**, 100797 (2022).
[42]K. C. Maurya, V. M. Shalaev, A. Boltasseva, and B. Saha, Opt. Mater. Express **10**, 2679 (2020).
[43]A. J. McAlister and E. A. Stern, Phys. Rev. **132**, 1599 (1963).
[44]G. M. Akselrod, J. Huang, T. B. Hoang, P. T. Bowen, L. Su, D. R. Smith, and M. H. Mikkelsen, Adv. Mater. **27**, 8028 (2015).
[45]H. Xu, L. Hu, Y. Lu, J. Xu, and Y. Chen, J. Phys. Chem. C **123**, 10028 (2019).
[46]Z. Zhang, Y. Mo, H. Wang, Y. Zhao, and S. Jiang, Appl. Opt. **58**, 4467 (2019).
[47]K. V. Sreekanth, M. Elkabbash, Y. Alapan, A. R. Rashed, U. A. Gurkan, and G. Strangi, Sci. Rep. **6**, 26272 (2016).
[48]B. Harbecke, B. Heinz, and P. Grosse, Appl. Phys. A **38**, 263 (1985).

Downloaded from http://pubs.aip.org/aip/apl/article-pdf/doi/10.1063/5.0150185/17923374/221704_1_5.0150185.pdf

Published under an exclusive license by AIP Publishing